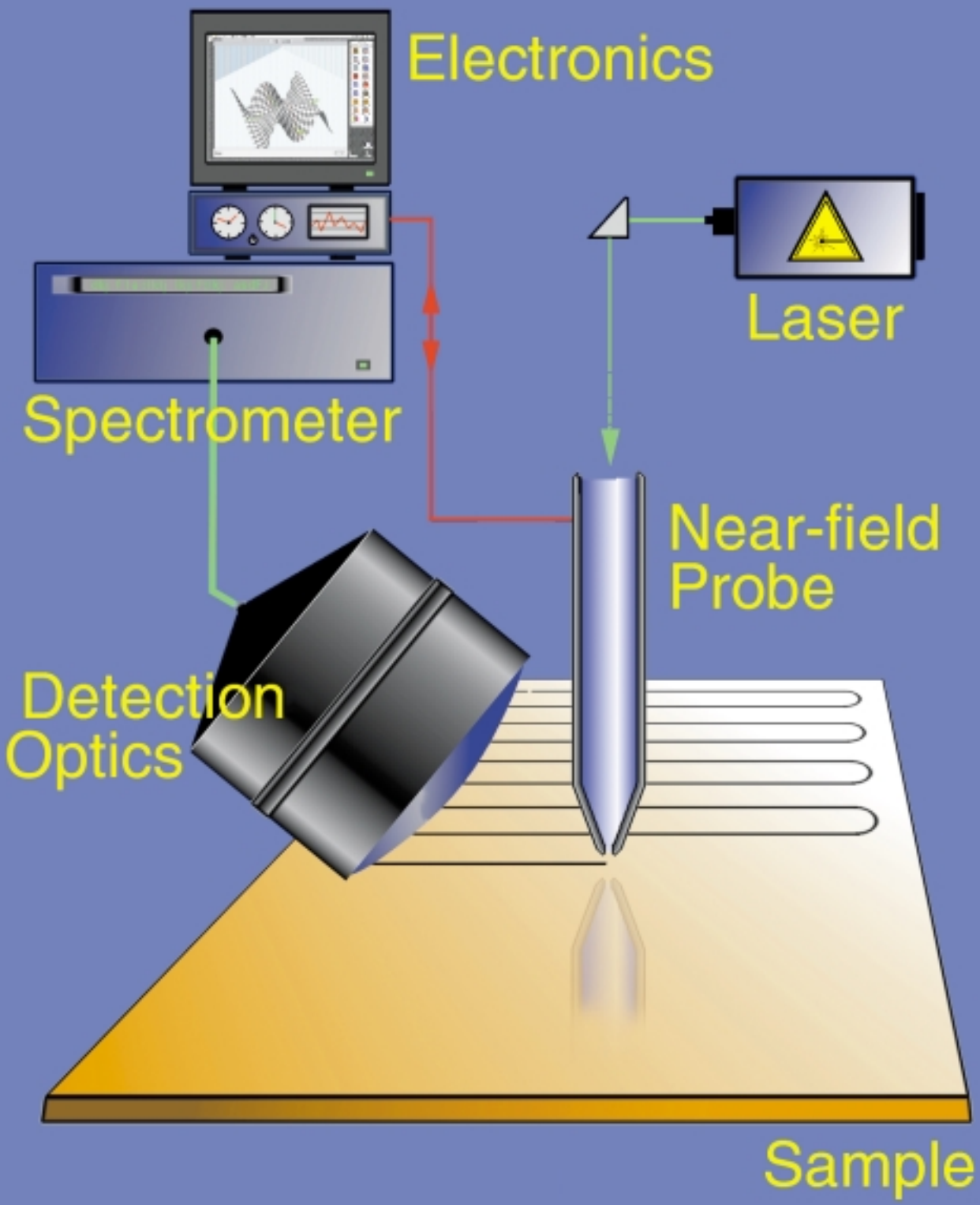

Scanning Near-Field Optical Microscopy and Spectroscopy as a Tool for Chemical Analysis

Renato Zenobi* and Volker Deckert

Research into the nanometer-scale region is currently of relevance in many branches of modern science and engineering, such as in microelectronics, supramolecular chemistry, and in a biological context. A great deal of attention is given to the design of molecular devices, usually towards understanding the function of existing "molecular machines". Central to this task are powerful diagnostic tools capable of recording chemical information with spatial resolution in the nanometer range. While elemental analysis of surfaces with a lateral resolution of a few dozen nanometers is almost routine, analysis of molecular species with a resolution of $< 1\ \mu m$ is very difficult. Scanning-tunneling and atomic-force microscopies usually do not give any chemical information. By combining scanning near-field optical microscopy (SNOM)—the "optical member" of the family of scanning-probe microscopies—with optical spectroscopy, it is possible to obtain molecular information from sample areas as little as 50 nm in diameter. In SNOM, a light source is scanned above the object of interest at a distance of a few nanometers. In the optical near field, the illuminated area is not subject to the Abbé diffraction limit, but merely by the size of the illuminating source. High quality SNOM probes can be reproducibly prepared by a chemical-etching method. These etched probes have an optical transmission up to 1000-fold higher than commercial (pulled) SNOM tips and can withstand higher laser power. This last advantage allows not only high resolution optical imaging, but also localized spectroscopic investigations of surfaces and even optical "nanosampling" by pulsed-laser ablation. The ablated material can be transported over a considerable distance, which opens the possibility for its subsequent analysis with a complementary, highly sensitive analytical method, such as mass spectrometry.

Keywords: analytical methods · mass spectrometry · optical near-field microscopy · optical spectroscopy · surface analysis

1. Introduction

A great breakthrough in surface science was the development of the scanning-probe microscopy techniques, led by the development of the scanning-tunneling microscope (STM), which earned Heinrich Rohrer and Gerd Binnig the 1986 Nobel Prize in Physics.[1–3] Soon thereafter, a host of related methods were developed, all based on piezoelectric scanning of a very sharp probe relative to the sample, such as atomic-force microscopy (AFM), scanning electrochemical microscopy, scanning magnetic microscopy, and many others. They are sometimes collectively referred to as the "children of the STM".[4]

[*] Prof. R. Zenobi, Dr. V. Deckert
Laboratorium für Organische Chemie
Eidgenössische Technische Hochschule (ETH) Zürich
Universitätsstrasse 16, 8092 Zürich (Switzerland)
Fax: (+41) 1-632-12-92
E-mail: zenobi@org.chem.ethz.ch

Of particular interest to applications in molecular science is scanning near-field optical microscopy (SNOM),[5–8] the "optical" version among the children of the STM. SNOM delivers light to spots of less than 100 nm diameter and thereby holds great promise for molecular analysis on the nanometer scale. An optical resolution of as little as 12 nm has been claimed by Betzig and Trautman[9] but only after deconvolution of the size of the near-field optical probe. This spatial resolution has not been reproduced lately by other researchers. Delivering light to such small spots is not possible by conventional optical methods, such as by a focussed laser beam. It is also impossible to resolve features separated by less than $\lambda/2$ by conventional optical microscopy, where λ is the wavelength of the illuminating light. This limitation is imposed by the Abbé diffraction limit. At visible wavelengths, a resolution approaching 200–250 nm should be theoretically possible but, except for confocal schemes employing oil-immersion lenses and therefore subject to other limitations, a resolution better than 0.5–1 μm is rarely achieved. This diffraction limit is the reason that short-wavelength ultra-

  1433-7851/00/3910-1747 $ 17.50+.50/0

violet light or even X-rays, where λ is smaller still, find increasing use in microelectronics and other applications of lithography but at the cost of more expensive optics and instrumentation.

The possibility of illumination in the visible, in the near ultraviolet, or in the infrared range onto a spot smaller than the diffraction limit permits the application of a wide range of spectroscopic methods to problems in chemistry, biology, materials science, and other fields in which the molecular composition of nanoscale objects is of interest. Analyzing the elemental composition with a resolution less than 100 nm is now established and a routine procedure with scanning Auger microscopy, some secondary-ion mass spectrometers, and certain forms of electron-microprobe analysis.[10] These methods typically operate under ultrahigh vacuum conditions, often require special sample pretreatment, and rely on focussing an ion or electron beam to a spot <100 nm in size, which is detrimental for most molecular species. The chemical analysis of the *molecular* composition with such a resolution was impossible in practise until now, and is just starting to be explored by a combination of SNOM technology with spectroscopic methods. A large advantage of the SNOM methods is that they can operate under atmospheric pressure.

2. Experimental Section

Commercially available near-field scanning optical microscopes (models Lumina and Aurora, ThermoMicroscopes (formerly Topometrix), Santa Clara, CA (USA) form the basic units of our instrumentation (Figure 1). Laser light penetrating through the nanometer-sized aperture of the probe illuminates the surface under investigation. The sample stage is scanned relative to the tip in order to maintain a fixed optical path. The emitted or scattered light from the sample is collected with high numerical aperture microscope objectives either in transmission or in reflection (not shown in Figure 1).

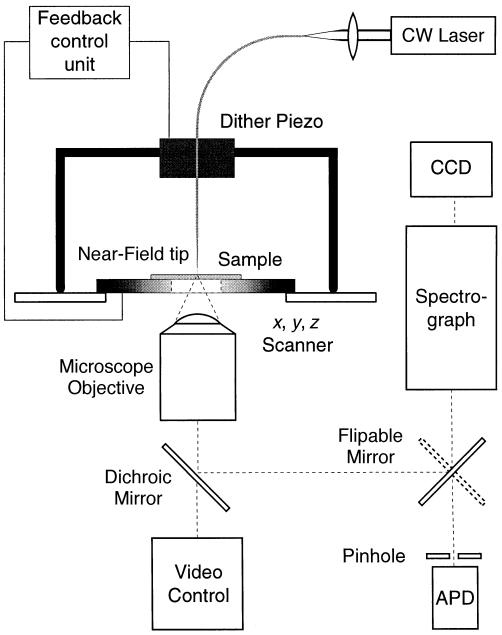

Figure 1. Equipment for scanning near-field microscopy. The sample is mounted on a piezoelectric *x*,*y*,*z* scanning stage. The SNOM tip is held either by a dither piezo (shown) or by a tuning fork (not shown). Shear force damping is used for controlling the tip–sample distance through a feedback loop. Light from a continuous-wave (CW) laser is coupled onto the blunt end of the fiber, illuminating the sample through the SNOM tip. Scattered light is collected either in transmission (shown) or in reflection (not shown) using conventional far-field optics. Detection uses either an avalanche photodiode (APD) or by an optical spectrograph equipped with a charge-coupled device (CCD). The entrance slit of the spectrograph or a pinhole mounted in front of the APD further reduce stray light.

Renato Zenobi is Professor of Analytical Chemistry at the Swiss Federal Institute of Technology (ETH) in Zürich (Switzerland). He is also one of the founders and the current chairman of the Center of Excellence in Analytical Chemistry at the ETH Zürich. He obtained his diploma from the ETH (1986) and his PhD degree from Stanford University (1990). After two postdoctoral appointments at the University of Pittsburgh and the University of Michigan (Ann Arbor), he returned to Switzerland in 1992. He held an Alfred Werner Fellowship at the Ecole Polytechnique Fédérale in Lausanne until 1994. He joined the faculty of the ETH Zürich in 1995. His research interests include laser-based analytical chemistry, laser-assisted mass spectrometry, and near-field optical microscopy and -spectroscopy.

R. Zenobi

V. Deckert

Volker Deckert is pursuing his Habilitation at the ETH Zürich. He obtained both his diploma (1991) and his PhD degree (1994) from the University of Würzburg (Germany), working in the area of Raman spectroscopy. He was a post-doc at the University of Tokyo and at the Kanagawa Academy of Science and Technology (1994/95) and worked on nonlinear and time-resolved laser spectroscopy. Since 1993, he has also been a freelancing developer of spectroscopy software for Photometrics, Tucson, AZ (USA). He joined the ETH Zürich in 1996 and is currently leading the Surface Analysis and Spectroscopy team in the group of Prof. R. Zenobi.

Collected light is then filtered and projected onto a sensitive detector for fluorescence detection or, alternatively, onto the entrance slit of an optical spectrograph. The latter is optimized for a greater amount of transmitted light. In our arrangement, a transmission holographic-grating spectrograph with a high numerical aperture was used (Holospec f/1.8i, Kaiser Optical Systems, Ann Arbor, MI (USA)).

To maintain a constant tip-to-sample distance, an optically detected shear-force feedback loop is most frequently used,[11, 12] although other methods have been employed.[13–17] For the feedback loop, the tip dithers at its resonance frequency. The dithering amplitude decreases dramatically when the tip is within 5–15 nm of the sample surface. The reasons for the shear force damping near the surface are still not fully understood; probably a combination of contact, frictional, and adhesive forces induced by a thin water film on the sample surface are responsible, at least under ambient conditions.[18, 19] In the "constant gap" mode, a feedback loop maintains a constant distance, normally < 10 nm, between the probe and surface. For flat samples, scans in "constant height mode" are advantageous to avoid topographic artifacts.[20] Such scans are performed in the absence of a distance feedback loop once the tip–sample distance has been established.

The probe is the most delicate component of any SNOM equipment. In this review, we will be dealing exclusively with "aperture SNOM probes", that is, tips with an apex smaller than the wavelength of the illuminating light, and made of a tapered glass fiber coated with metal except at the apex.[12, 21] Other probes are also used, including point-source emission probes[22] or apertureless probes.[23–28] The important properties of aperture SNOM probes are good transparency, a well defined circular aperture, no light leaking through defects in the metal coating, and a high optical-damage threshold. Several methods have been proposed to prepare the tapered glass core probes. Adiabatic pulling of optical fibers during heating with a CO_2 laser,[29, 30] similar to preparing a pipette, is currently the most popular method. In another case, tiny splinters of glass as tetrahedral SNOM tips are used.[31, 32] Several groups are employing focused ion-beam milling to create very well defined apertures at the tip apex.[33, 34] Recently, microfabricated tips have been described in the literature[35–38] and such tips will become commercially available soon.

A very practical method for the preparation of probes is based on etching glass fibers at the meniscus between hydrofluoric acid (etching fluid) and a protective organic overlayer.[39] Etched fiber probes usually provide a higher optical throughput due to larger cone angles than the pulled probes,[38–42] but a high yield of good tips produced by etching is often not obtained. A more reproducible and efficient method, called "tube etching", was recently developed in our laboratory.[43] By this method, the protective polymer coating of the optical fiber is retained, and a tip forms due to a convective mechanism inside the polymer jacket. The method is tolerant to perturbations during preparation such as vibrations and temperature changes. The resulting tips are produced reproducibly and in high yield with large cone angles and smooth aluminum coating. It should also be noted that the composition of the glass is crucial for obtaining good etching results and also to avoid large background signals during SNOM experiments arising, for example, by Raman scattering of the fiber material itself (see Section 3.2).

The left side of Figure 2 shows an electron micrograph of an aluminum-coated SNOM tip produced by the tube-etching method. The large opening angle is immediately apparent

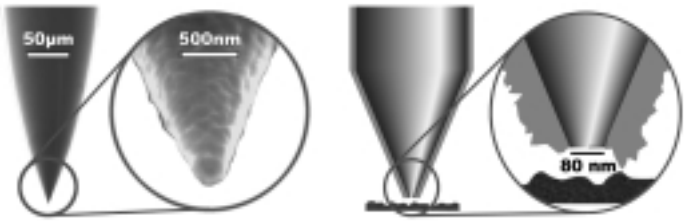

Figure 2. Left: Electron micrograph of a SNOM tip produced by the tube-etching method and a closeup of the apex region of the same tip. Right: Representation of the origin of differences between optical and topographic images.

and, in the closeup, an aperture of well below 100 nm diameter is visible. On the right side, the difference between the "topographic tip" and the "optical tip" is illustrated. Sometimes a grain of the metal coating will protrude such that the center of the tapered optical fiber and that of the topographic tip can be separated by several tens of nanometers. If this is the case, the offset of the topographic and the optical images can lead to a misinterpretation of the combined SNOM and topographic data.

3. Results and Discussion

3.1. Fluorescence Imaging with Etched Optical-Fiber Tips

Fluorescence is by far the most widespread and easily implemented mode for chemical imaging by near-field optical methods, although the resolution offered by modern confocal fluorescence-microscopy techniques is often sufficient.[44] A fluorescent tag must be attached to the molecules of interest, unless their natural fluorescence can be exploited. Due to high signal intensity, it is even possible to image single fluorescent molecules with SNOM technology. Fascinating applications, involving single molecule fluorescence detection, have been described by Betzig,[45] Xie,[46–48] and van Hulst.[49]

A very promising area for the use of SNOM in combination with fluorescence detection is the study of biological nanostructures, in particular, parts of cells. An example from our laboratory is shown in Figure 3A. In this application, dog kidney (Madine–Darby canine kidney, MDCK) cells were grown on a flat silica slide using glutaraldehyde and lysed such that the interior of their cell walls became accessible to SNOM imaging.[50] The actin filaments of the cytoskeleton were stained selectively with a rhodamine-labeled phalloidin; they appear green in the image.

Figure 3 shows immediately that much finer features are resolved with SNOM. Specialized laser-scanning confocal-

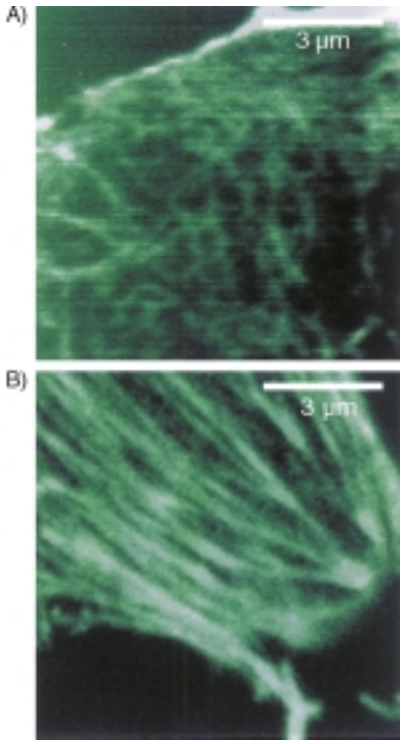

Figure 3. A) SNOM fluorescence image of the cytoskeleton of Madine–Darby canine kidney cells stained with a fluorescent dye (see text for details). B) Confocal micrograph image of the same sample (different area).

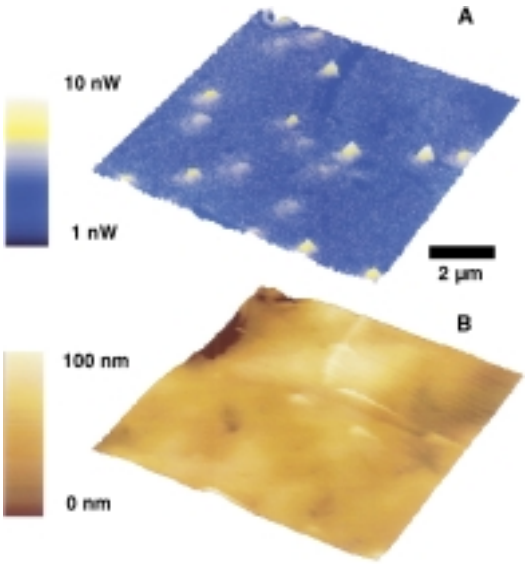

Figure 4. A) SNOM/fluorescence image and B) topographic image of a 10×10 µm area of a PVB film containing fluorescent microspheres. The spheres had a diameter of 288 nm. The fluorescence was excited with the 488 nm line of an Ar-ion laser.

microscopy techniques push the resolution below 200 nm by, for example, using two-photon excitation. However, the lateral resolution in Figure 3B is about 300 nm, typical for confocal fluorescence microscopes. Actin filament bundles can be resolved by confocal microscopy but the resolution in the SNOM image (Figure 3A) considerably exceeds that of the confocal-microscope image (Figure 3B).

Near-field optical detection is not strictly limited to surfaces. This is illustrated in Figure 4. Here, a sample consisting of fluorescent latex spheres embedded in a polyvinyl butyral (PVB) thin film was imaged by SNOM using fluorescence detection in transmission mode. The spheres had a diameter of 288 nm and were impregnated with a fluorescent dye that is easily excited with the 488 nm line of an Ar-ion laser. Spheres that are located on the surface of the polymer matrix appear with sharp contours both in the topographic and in the SNOM/fluorescence image, albeit with a larger apparent diameter of about 375 nm. This allows determination of the tip diameter by deconvolution, in this case an optical tip diameter of ≤ 100 nm may be deduced.

Other latex spheres appear blurred in the optical image at locations where no protrusions were apparent in the simultaneously recorded topographic image. This can be attributed to latex spheres that are not located directly at the surface but are embedded deeper in the PVB film. Detection to a depth of at least 150 nm is therefore possible.

A disadvantage of fluorescence imaging is the need for a fluorescent moiety or tag to be employed, which is not always possible. A further shortcoming is that fluorescence spectra are broad and structureless, to reveal little chemical information. It would be, at best, very difficult to identify unknown molecules based solely on fluorescence. Other optical spectroscopies are better suited for this purpose.

3.2. Near-Field Vibrational Spectroscopy

Vibrational spectroscopy is very useful to identify unknown molecules due to its high chemical-information content. It is, however, difficult to combine infrared spectroscopy with SNOM for two reasons: 1) Fiber materials in the mid-infrared region, where most molecular vibrations are detected, are not readily available and are difficult to handle; 2) The discrepancy between the desired resolution and the diffraction limit is accentuated due to the much longer excitation wavelength. Nevertheless, there are some very interesting, even heroic, attempts to use SNOM methods for imaging the mid-infrared range.[51] Keilmann et al.[28] and Boccara et al.[25, 26] use an apertureless approach: An AFM tip is used for field enhancement within the focus of a fixed-frequency infrared laser. A resolution of $\lambda/600$, about 17 nm, was claimed with this approach.[25] However, true IR spectroscopy with a resolution on the order of a few nanometers has not been achieved yet.

An alternative to IR spectroscopy is Raman spectroscopy. The difficulty lies here with the exceedingly low scattering cross-section, such that its combination with SNOM seems hopeless at first. However, there are certain advantages of Raman over IR spectroscopy: Suitable optical fibers are readily available, there is a large choice of very sensitive detectors, and it is possible to use resonance-excitation techniques. Finally, Raman cross-sections are increased by orders of magnitude if surface enhancement (SERS) is employed. It is relatively straightforward to combine surface-enhanced spectroscopies with SNOM to improve the overall photon yield.

Several research groups have begun to implement Raman microscopes where the excitation uses an aperture SNOM probe.[52–62] The alternative is again to use apertureless probes: A very sharp tip, usually a metallic STM or AFM tip, can be used for field enhancement inside the diffraction-limited focus of the illuminating laser beam. The position of the tip can be temporally modulated in order to employ lock-in detection schemes.[23, 24] Resolution to 10 Å has been claimed using this method, albeit not with Raman scattering. It is, however, still unclear where the optical contrast originates from. For example, it is possible that light reflected off the side of the probe contributes more to the overall signal than radiation from the apex of the probe. A shadowing effect can also occur, which may even cause a reversal of the optical contrast. Clever schemes, for example using two-photon excitation, can be used to circumvent these problems.[27]

Figure 5 shows an image of a silver SERS substrate that was specially designed to contain isolated islands of silver without any topographic substructure.[63] The substrate was then coated with an adlayer of rhodamine 6G (R6G). First, the surface morphology was measured using the shear-force feedback-loop mechanism. The SNOM probe was then parked at selected positions of the depicted 1×1 μm area and the Raman spectrum of the R6G layer was measured. Each measured position in Figure 5 is depicted by a white circle, the diameter of which (about 70 nm) indicates the approximate optical resolution obtained by the SNOM tip. Each position was illuminated for one minute through the SNOM tip, to yield the characteristic Raman spectrum of R6G. The optical resolution of the tip was determined by inherent spectral variation in the Raman spectra of adjacent locations; scanning electron micrographs of the used SNOM tips confirmed this estimate of 70 nm. Assuming a monolayer coverage of the dye, a spot size of this diameter corresponds to a sensitivity of less than 100 R6G molecules!

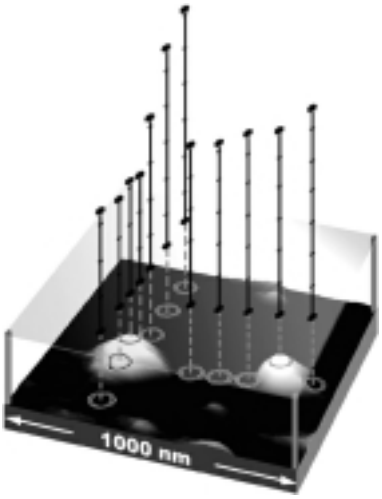

Figure 5. Shear-force topographic image of a substrate with a SERS coating. For near-field Raman measurements, a monolayer of rhodamine 6G is applied. At various locations, marked by the circles, near-field SERS measurements were made. The circles are 70 nm in diameter and represent the optical resolution obtained with the SNOM tip. The pole heights above the transparent plane denote the relative signal intensity of the Raman peak at 1650 cm^{-1}. The signals are normalized against the average Raman intensity measured on unmetallized glass slides. Each segment of the poles corresponds to an 1000-fold signal enhancement.

As a measure for the Raman enhancement factor (EF), the normalized and background-corrected Raman peak intensities at 1650 cm^{-1} were selected, which correspond to an aromatic C–C stretch vibration of R6G. The magnitude of this band was directly compared with the average value obtained for unmetallized, R6G-coated substrates. The calculated EFs are superimposed on the topographic image of Figure 5. Each segment of the poles corresponds to an additional 1000-fold signal enhancement. The EFs lay between 2000 to well above 6000, with over a 50% variation observed in the Raman intensity for two points separated by less than 100 nm. Interestingly, the overall EF measured by far-field optics was higher still, around 11 000. We still cannot fully explain the discrepancy between the enhancement factors determined by near-field and far-field measurements. Perhaps "hot spots" with much higher EFs exist on the substrate, which cannot be found in the near field. Alternatively, cumulative effects of neighboring islands may play a role. A further possibility is that the aluminum coating of the SNOM tip deteriorates the EF near the silver islands by some electrostatic interaction as soon as the SNOM tip is in proximity.

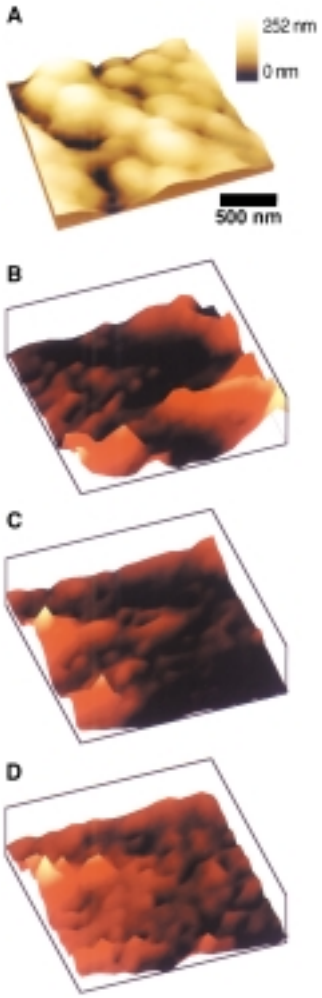

Figure 6. SNOM-SERS imaging of a BCB-labelled DNA sample deposited on a substrate consisting of monodisperse silver spheres for SERS enhancement. Lateral dependence of: A) shear-force topography; B) the Raman signal intensity at 800 cm^{-1} (glass); C) the near-field surface-enhanced Raman intensity at 1641 cm^{-1} (BCB) before normalization; and D) the near-field surface-enhanced Raman intensity at 1641 cm^{-1} after normalization. In images (B)–(D), the pixel size was only 100×100 nm and, for each graph, the intensity of one line of the complete Raman spectrum was plotted. In images (C) and (D), the contrast between the lowest and the highest Raman intensity was about a factor of three.

We have also demonstrated high resolution Raman imaging is possible with the near-field optics. Figure 6A shows the shear-force topograpic image and Figure 6B–D the optical images of a 2×2 μm area of a SERS-coated substrate, which consisted of silver-coated Teflon microspheres with an overall diameter of 300 nm.[61] The shear-force topography im-

age shows that aggregated silver spheres are clearly resolved and their spatial distribution is quite irregular. This substrate was coated with a monolayer of a 18-mer DNA fragment labelled with brilliant cresyl blue (BCB).[62] To achieve a reasonable acquisition time for the entire image, we measured the near-field Raman spectra as an array of only 20×20 data points. This acquisition time was twenty times longer compared to normal SNOM imaging times. Nevertheless, for an aperture smaller than 100 nm, it is the tip size and not the step size that limits the optical resolution. This represents a slight undersampling that we accept in order to obtain the entire spectral information within a reasonable measurement time. The image of the Raman spectrum feature at 800 cm^{-1} (Figure 6B), which stems from the glass of the SNOM tip itself, is at least partially dependent upon the topography. From the comparison of Figures 6A and B, it is obvious that the correlation of the topographic information and the reflected light from such a highly corrugated sample is by no means trivial. In particular, an interpretation of the image and an estimation of the optical resolution is difficult if topographic coupling or shadowing effects[20] occur.

The image in Figure 6C shows the lateral intensity dependence of the Raman band from the BCB label (at 1641 cm^{-1}). By comparing Figures 6B and 6C, it is apparent that Raman signals from the label and from the glass tip show some correlation, such as the increased intensity in the lower left corner. However, the Raman signal stems from the BCB-labelled DNA, whereas the glass scattering signal originates entirely from the SNOM tip. The bands from the glass therefore should be proportional to the local reflectivity of the surface. The Raman scattered signal is subject to the same reflectivity changes as the glass signal. If, for instance, a particle between the illuminated spot and the collection optics decreases the reflectivity, the Raman signal is attenuated in exactly the same fashion and extent. In other words, the topography of our sample is encoded in the reflectivity signal, such that the topographic effects can be removed from the Raman signal by normalizing it against the intensity of the glass band. The effect of this normalization is demonstrated in Figure 6D, in which the Raman intensity of the 1641 cm^{-1} BCB band at each position after dividing the data in Figure 6C by the intensity of Figure 6B. A comparison of Figures 6D and 6C shows that instead of two bright spots, the corrected image shows only one spot of high SERS intensity. At the position in the lower left, an enhanced sample reflectivity is responsible for the increased Raman signal, whereas the bright spot on the upper left remains after the normalization.

In the corrected Raman images at all frequencies, we observe a small, highly SERS-active region of about 400 nm diameter on the center-left side of the image. If we assume a uniform distribution of the sample on the surface, this increase in intensity can only be attributed to a particularly strong enhancement by the substrate ("hot spots"), although concentration fluctuations leading to a variation of Raman signals cannot entirely be excluded. Interestingly, the maximum SERS enhancement does not coincide with the position of a silver particle but, in fact, the location of the maximum enhancement seems to be at a position where a gap between the silver spheres is visible (Figure 6A). We have to be aware of the possibility that the topographic and the SNOM-Raman image may not be in perfect congruence. It has been postulated that "hot spots" may be located on SERS substrates where gaps or cavities exist.[64] In previous work by Emory and Nie,[56] there are hints for such "hot spots" but they were unable to image these sites directly. In contrast, the SNOM method allows directly visualization of "hot spots" because of the simultaneous recording of sample topography and Raman intensity at each data point; this is particularly straightforward if low-density silver-island films are used as SERS substrates.[63]

It is interesting to compare the relative magnitude of Raman scattered light and fluorescence signals. The cross sections found for SERS on "hot spots" was of the same order of magnitude as that of the fluorescence signals![56, 65] Upon absorption of a single photon, an individual molecule will either undergo a Raman scattering event or fluoresce, but not both. Photobleaching processes are intimately linked with fluorescence and therefore should not affect the Raman emission process. This is demonstrated in Figure 7, where three consecutive spectra of R6G deposited on a silver-island SERS substrate are shown. The intensity of the fluorescence background decreases due to photobleaching, while that of the Raman bands remains constant, in agreement with the expectation. The reason for this behavior may be that "hot spots" on the SERS substrate coax the adsorbed molecules into undergoing Raman scattering rather than fluorescence, thereby protecting them from photobleaching. The average coverage of the SERS substrate by the dye was slightly more than one monolayer; apparently only a fraction of the adsorbed R6G molecules are associated with these protective sites but are responsible for quite strong SERS signals. This again supports the idea that only a few "hot spots" exhibit a very large Raman enhancement and are responsible for the overall intensity observed.

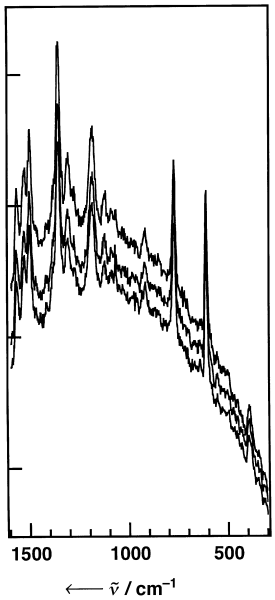

Figure 7. Raman lines superimposed on a fluorescence background in the optical spectrum of a monolayer of rhodamine 6G deposited on a silver SERS substrate (excitation at 488 nm). The spectra were recorded consecutively (from top to bottom), using an integration time of 5 min per spectrum. Slow photobleaching is observed for the fluorescence background, while the intensity of the Raman lines remains constant.

Are SERS methods the only hope to obtain Raman spectra excited by near-field optical probes? The answer to this question is, as demonstrated in Figure 8, a clear "no". The near-field Raman spectrum of a chemical-vapor deposited (CVD) diamond film shows a sharp feature at 1330 cm^{-1}, which is the well known Raman band of diamond. Raman scattering from graphitic carbon is expected around

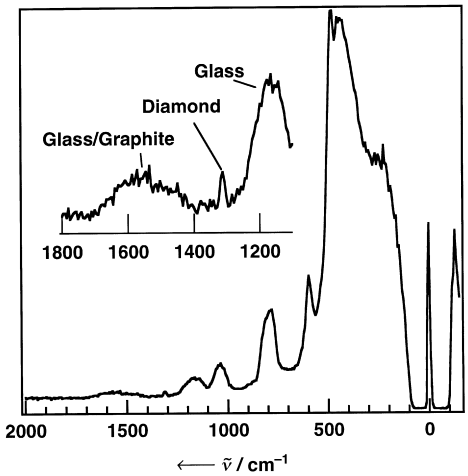

Figure 8. Near-field Raman spectrum of a diamond film produced by CVD methods. The excitation wavelength was 488 nm and the laser line was filtered out in front of the spectrograph by a holographic notch filter. Strong bands due to Raman scattering from the SERS tip itself dominate the spectrum (glass). Inset: the sharp band at 1330 cm^{-1} is assigned to diamond, and the broad feature at $\approx$1600 cm^{-1} is due partially to glass and partially to graphitic carbon.

1600 cm^{-1}, but unfortunately a fairly strong residual signal from the long progression of glass Raman bands, originating from the tip itself, overlaps with the sp^2 carbon band. This is partially due to the low Raman intensity of the sample, but the Raman emission from the glass of the SNOM tip depends strongly on the glass fiber material used. Our latest generation of SNOM tips exhibit much lower Raman scattering in this spectral region, such that, in principle, the purity of the film could be measured at any given location.

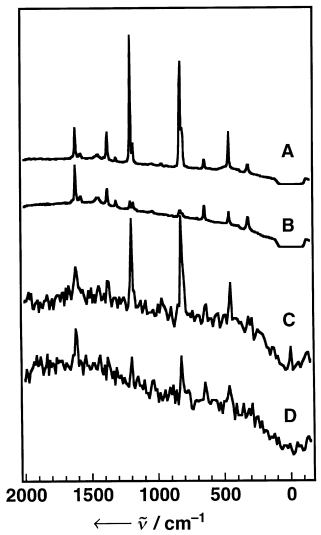

Figure 9. Raman spectra recorded in liquid *p*-xylol using polar-filtered exciting light and detection. A) Far-field spectrum with parallel polarizers; B) Far-field spectrum with perpendicular polarizers; C) Near-field spectrum with parallel polarizers; D) Near-field spectrum with perpendicular polarizers. The absolute intensities for each spectrum are not directly comparable. The laser power was 10 μW (at $\lambda =$ 488 nm) and the signal, averaged over 10 min, was used.

The exquisite resolution in the *z* direction makes the SNOM an attractive tool to study the interface between two liquids. In particular, molecular orientation at such interfaces may be studied by the anisotropies of the Raman scattering tensor using polar-filtered exciting light and detection. For the isotropic part of the scattering tensor of the fully symmetric vibrational modes, a strong decrease in signal intensity is expected if the polarizers are crossed. In contrast, for anisotropic modes, some intensity will still be detected even for crossed polarizers. This is illustrated in Figure 9. At an interface, the orientation of the investigated molecules will not be randomly oriented and the structure of an interface can be studied through symmetry considerations.

Figure 9A and 9B are far-field Raman spectra of liquid *p*-xylol, while 9C and 9D are near-field Raman spectra of the same. Over the transition from parallel to crossed orientation of the polarizers in the excitation and detection beam path, the expected intensity decrease is observed for many Raman modes, for example, the strong aromatic-ring vibrations at 820 and 1200 cm^{-1}. In contrast, the band at about 1600 cm^{-1} remains strong even when crossed polarizers are used, indicating large anisotropic components in its scattering tensor. Figure 9 shows impressively that the SNOM tip used for recording the near-field data preserves the polarization quite well.

3.3. Laser Ablation through SNOM Tips

The high transmission SNOM tips that we use permit not only high resolution optical imaging and spectroscopic investigations of surfaces, but also optical "nanosampling" by pulsed-laser ablation through the tip.[66] The laser-ablated material can be transported over a considerable distance and analyzed in a second step by a highly sensitive analytical method such as mass spectrometry. A schematic of this concept is shown in Figure 10.

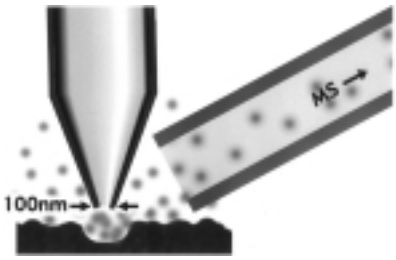

Figure 10. Schematic representation of the coupling of laser ablation through the SNOM tip with mass-spectrometric analysis of the vaporized material.

This localized ablation has already been described and a crude realization has appeared in the literature.[67] The authors guided a sharpened optical fiber over a transmission electron microscopy (TEM) grid inside the ion source of a mass spectrometer and performed a matrix-assisted laser-desorption/ionization (MALDI) mass-spectrometry experiment. The TEM grid was covered with an acetylcholine sample embedded in a 2,5-dihydroxybenzoic acid matrix. The advantage of this experiment over earlier MALDI studies, where the laser light was also brought in by an optical fiber,[68, 69] remains unclear. The spatial resolution was of several micrometers, far greater than what is possible with the SNOM method.

Several mechanisms are possible for laser-induced ablation through SNOM tips.[70] The photochemical mechanism assumes that the energy is deposited in the sample via optical absorption and ablation follows as a consequence of breaking chemical bonds. The photothermal mechanism is similar but assumes the absorbed optical energy would be converted into

heat, which causes ablation from the locally heated spot. A ballistic mechanism is also possible, in which the material from the tip is sputtered onto the sample and material ablates from the surface. A ballistic mechanism is the most likely explanation for an experiment carried out on an anthracene surface using a completely metallized SNOM tip,[41] since, in this case, no photons reach the sample and therefore a sputter process, either by metal atoms from the tip or by material adsorbed on its surface, was believed to be the reason for the ablation process. Fourth, one also has to take transient thermal expansion[71–73] into account as a possible mechanism for the creation of surface indentations, but it is likely to be negligible.[70]

We now discuss an experiment that gave clear results about the ablation mechanism of a rhodamine B film. The sample was irradiated with laser pulses either at its optical adsorbtion maximum ("on resonance", 532 nm) or nearby this point ("off resonance", 650 nm). SNOM tips with apertures of <100 nm diameter were used. No significant difference in the optical transmission of the SNOM tip over the 400 to 650 nm range, although some decrease is expected with an increasing difference between the wavelength and tip aperture size. Figure 11 shows shear-force topographic images recorded after several laser pulses had been fired onto the sample. No ablation was observed for the off-resonance wavelength (Figure 11 A; $\lambda = 650$ nm, 2.1 μJ per pulse). In contrast, well defined, ≈ 70 nm diameter (FWHM), 5 nm deep holes were created when the laser operated at a wavelength that is strongly absorbed by the sample (Figure 11 B; $\lambda = 532$ nm, 1.4 μJ per pulse). This clearly points to an optical ablation mechanism, either photochemical or photothermal. Energy transfer by absorption of photons appears to be more efficient than by a ballistic process. The photon energy used here is not sufficient for inducing bond dissociation in rhodamine molecules, in contrast to ablation experiments with ultraviolet laser radiation, where photochemical dissociation is often used to rationalize the observed phenomena.[74] We therefore suggest that a photothermal mechanism is responsible for the ablation of the rhodamine film: The absorbed photon energy is converted to vibrational excitation, which causes a rapid temperature increase and leads to thermal desorption of the molecules.

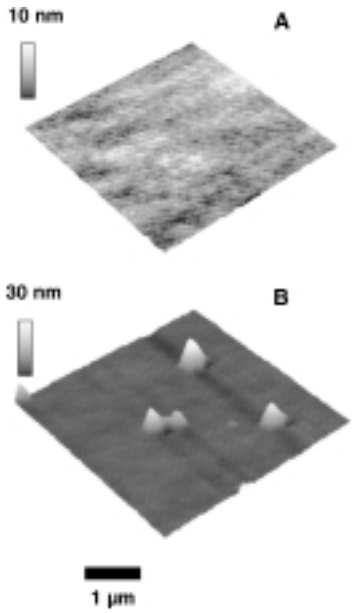

Figure 11. Shear-force topographic images of a rhodamine B film after transmitting laser pulses through the SNOM tip at A) 2.1 μJ at $\lambda = 650$ nm, far from the maximum absorption of rhodamine B, and B) 1.4 μJ at $\lambda = 532$ nm (B), a wavelength near the maximum absorption. The total topographic contrast in the z direction is A) 10 nm and B) 30 nm.

Another interesting observation in Figure 11 is that the ablated material is redeposited on the sample surface close to the ablation crater. The distribution of redeposited material was not symmetric in this experiment but was always to the left side of the crater and independent of the scan direction. In other SNOM ablation experiments, the distribution was more symmetric. The origin of the directionality appears to be the tip itself: The apex of a SNOM tip is frequently not symmetric and the ablated material is ejected in a specific direction.

Transport over micrometer distances was observed in several cases. The result of such an experiment is shown in Figure 12.[70] Here, an anthracene crystal surface was continuously irradiated with a pulsing laser (6 ns, 532 nm, 50 μJ) operated at a 20 Hz repetition rate over a 1×2 μm area. A shear-force image of a larger area was then recorded without irradiation. An approximately 1 μm wide trench with well defined edges could be detected in the upper-left corner of the image, while a 2 μm wide, 60 nm high mound was found about 5 μm away running roughly parallel to the trench. We interpret this again as vaporization followed by redeposition of material in a preferred direction. The direction of deposition is most likely determined by an asymmetry of the tip. For collection of ablated molecules, for example by a vacuum interface to a mass spectrometer, this asymmetry could be an advantage if the SNOM tip could be arranged to direct the ablated material towards the collector.

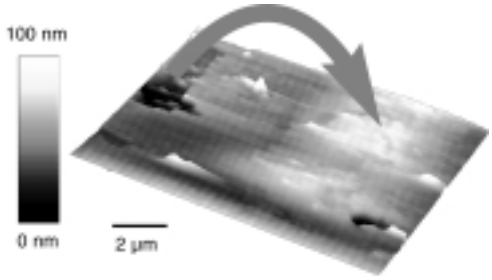

Figure 12. Transport of material over many micrometers: A topographic image of a 5×8 μm area of an anthracene film crystal surface, previously irradiated in a 1×2 μm trench in the upper left corner with ablating laser pulses (pulse: 6 ns pulse; wavelength: 532 nm; pulse energy: 50 μJ; repetition rate: 20 Hz). Total topographic contrast in the z direction is 100 nm. Adapted from ref. [70].

From Figure 12 we also estimate that only a few, larger chunks of material are ablated. Most of the anthracene is found in the form of a diffuse and structureless mound, which is expected if the molecules are redeposited from the gas phase. We have also shown that the laser-ablated molecules do not decompose.[70] We conclude that material transport does not take place by a mechanical dragging from the SNOM tip, but instead by vaporization and redeposition in a direction dictated by the assymetry of the tip.

4. Conclusions and Outlook

Near-field imaging based on aperture probes can now provide spectroscopic data with a lateral resolution on the

order of 50 nm. Some improvements in resolution may still be feasible but the aperture SNOM will probably never reach a resolution of 1 nm or less, which is possible by STM and AFM. However, as shown in this article, SNOM can provide a wealth of chemical information, which, in our opinion, more than compensates for the lack in spatial resolution.

High quality, high transmission SNOM tips can now be produced by various methods. The chemical etching method described here is one of the most easily implemented and provides high quality SNOM tips in a good yield. The "tube etched" tips can also withstand higher laser energies[75] and are therefore brighter near-field light sources.

We have shown examples of fluorescence and SERS imaging in the optical near-field with a lateral optical resolution of less than 100 nm, relatively short exposure times, and high signal-to-noise ratios. The different origins of the reflectivity and Raman signals can be used for an intensity correction of the Raman images by a simple normalization. This procedure corrects topographic artifacts present in standard SNOM images and can always be used if the detection of the interesting compound can be made at a different wavelength.

Surface enhancement of optical transitions appears to be due to a small number of "hot spots". With the combined optical and topographic information available in SNOM, we have a good chance to identify the nature of these sites. Surface enhancement, however, is not always a prerequisite for obtaining near-field Raman spectra, as shown on the example of a CVD diamond film. Finally, the tip itself could be used as a platform to carry a small particle[76, 77] that provides strong Raman enhancement. Such a "tip SERS" approach would not require the sample to be deposited on a rough silver film and thereby makes the technique more generally usable.

In the area of pulsed-laser ablation through SNOM tips, we have shown that it is possible to create highly localized (around 70 nm diameter) ablation craters on the surface of organic materials. The ablated molecules remain intact and often fly in a direction determined by an asymmetry of the SNOM tip. Material can be transported over several micrometers, collected, and analyzed by a complementary method. We have recently built an interface to a mass spectrometer for this purpose. In contrast to common laser-ablation ion sources for mass spectrometry, this interface allows the sample to be at ambient pressure. Mass spectral data of material ablated by single diffraction-limited laser pulses have been successfully recorded, and the signal-to-noise ratio was good enough to put an equivalent near-field experiment within reach.

We wish to thank Dr. Dieter Zeisel for many contributions to this article, Dr. Yung Doug Suh, Raoul Stöckle, Christian Fokas, Anja Vinckier, Urs Ziegler, Dr. Roland Hauert, Dr. Jörg Patscheider, and Dr. Tuan Vo-Dinh for their help, and the Swiss National Science Foundation for financial support (National Research Project "Nanotechnology", NFP-36).

Received: July 21, 1999 [A 355]

[1] G. Binnig, H. Rohrer, *Helv. Phys. Acta* **1982**, *55*, 726 – 735.
[2] G. Binnig, H. Rohrer, C. Gerber, E. Weibel, *Phys. Rev. Lett.* **1982**, *49*, 57 – 59.
[3] G. Binnig, H. Fuchs, C. Gerber, H. Rohrer, E. Stoll, E. Tosatti, *Europhys. Lett.* **1986**, *1*, 31 – 36.
[4] R. Pool, *Science* **1990**, *247*, 634 – 636.
[5] D. W. Pohl, W. Denk, M. Lanz, *Appl. Phys. Lett.* **1984**, *44*, 651 – 653.
[6] A. Lewis, M. Isaacson, A. Harootunian, A. Muray, *Ultramicroscopy* **1984**, *13*, 227 – 231.
[7] D. W. Pohl, U. C. Fischer, U. T. Dürig, *Scanning Microscopy Technologies and Applications*, Washington, DC, **1988**, pp. 84 – 90.
[8] E. Betzig, M. Isaacson, A. Lewis, K. Lin, *Scanning Microsc. Technol. Appl.* **1988**, *897*, 91 – 99.
[9] E. Betzig, J. K. Trautman, *Science* **1992**, *257*, 189 – 195.
[10] D. Brune, R. Hellborg, H. J. Whitlow, O. Hunderi, *Surface Characterization*, WILEY-VCH, Weinheim, **1997**.
[11] R. Toledo-Crow, P. C. Yang, Y. Chen, M. Vaez-Iravani, *Appl. Phys. Lett.* **1992**, *60*, 2957 – 2959.
[12] E. Betzig, P. L. Finn, J. S. Weiner, *Appl. Phys. Lett.* **1992**, *60*, 2484 – 2486.
[13] M. Garcia-Parajo, E. Cambril, Y. Chen, *Appl. Phys. Lett.* **1994**, *65*, 1498 – 1500.
[14] K. Karrai, R. D. Grober, *Ultramicroscopy* **1995**, *61*, 197 – 205.
[15] J. W. P. Hsu, M. Lee, B. S. Deaver, *Rev. Sci. Instrum.* **1995**, *66*, 3177 – 3181.
[16] J.-K. Leong, C. C. Wiliams, *Appl. Phys. Lett.* **1995**, *66*, 1432 – 1434.
[17] J. Barenz, O. Hollricher, O. Marti, *Rev. Sci. Instrum.* **1996**, *67*, 1912 – 1916.
[18] H. Heinzelmann, D. W. Pohl, *Appl. Phys. A* **1994**, *59*, 89 – 101.
[19] C. Durkan, I. V. Shvets, *J. Appl. Phys.* **1996**, *80*, 5659 – 5664.
[20] B. Hecht, H. Bielefeldt, Y. Inouye, D. W. Pohl, L. Novotny, *J. Appl. Phys.* **1997**, *81*, 2492 – 2498.
[21] D. W. Pohl, *Adv. Opt. Electron Microsc.* **1991**, 243 – 312.
[22] N. Kuck, K. Lieberman, A. Lewis, *Appl. Phys. Lett.* **1992**, *61*, 139 – 141.
[23] F. Zenhausern, M. P. O'Boyle, H. K. Wickramasinghe, *Appl. Phys. Lett.* **1994**, *65*, 1623 – 1625.
[24] F. Zenhausern, Y. Martin, H. K. Wickramasinghe, *Science* **1994**, *269*, 1083 – 1085.
[25] A. Lahrech, R. Bachelot, P. Gleyzes, A. C. Boccara, *Opt. Lett.* **1996**, *21*, 1315 – 1317.
[26] A. Lahrech, R. Bachelot, P. Gleyzes, A. C. Boccara, *Appl. Phys. Lett.* **1997**, *71*, 575 – 577.
[27] E. J. Sánchez, L. Novotny, X. S. Xie, *Phys. Rev. Lett.* **1999**, *82*, 4014 – 4017.
[28] B. Knoll, F. Keilmann, *Nature* **1999**, *399*, 134 – 137.
[29] E. Betzig, J. K. Trautman, T. D. Harris, J. S. Weiner, R. L. Kostelak, *Science* **1991**, *251*, 1468 – 1470.
[30] G. A. Valaskovic, M. Holton, G. H. Morrison, *Appl. Opt.* **1995**, *34*, 1215 – 1228.
[31] U. C. Fischer, J. Koglin, H. Fuchs, *J. Microsc.* (*Oxford*) **1994**, *176*, 231 – 237.
[32] J. Koglin, U. C. Fischer, H. Fuchs, *J. Biomed. Opt.* **1996**, *1*, 75 – 78.
[33] J. A. Veerman, A. M. Otters, L. Kuipers, N. F. van Hulst, *Appl. Phys. Lett.* **1998**, *72*, 3115 – 3118.
[34] S. Pilevar, K. Edinger, W. Atia, I. Smolyaninov, C. Davis, *Appl. Phys. Lett.* **1998**, *72*, 3133 – 3135.
[35] S. Münster, S. Werner, C. Mihalcea, W. Scholz, E. Oesterschulze, *J. Microsc.* **1997**, *186*, 17 – 22.
[36] W. Noell, M. Abraham, K. Mayr, A. Ruf, J. Barentz, O. Hollricher, O. Marti, P. Günther, *Appl. Phys. Lett.* **1997**, *70*, 1236 – 1238.
[37] D. Drews, W. Noell, W. Ehrfeld, M. Lacher, K. Mayr, O. Marti, C. Serwatzy, M. Abraham, *SPIE Conference on Materials and Device Characterization in Micromachining*, Santa Clara, CA, **1998**, pp. 76 – 83.
[38] T. Yatsuia, M. Kourogi, M. Ohtsu, *Appl. Phys. Lett.* **1998**, *73*, 2090 – 2092.
[39] P. Hoffmann, B. Dutoit, R.-P. Salathé, *Ultramicroscopy* **1995**, *61*, 165 – 170.
[40] L. Novotny, D. W. Pohl, B. Hecht, *Opt. Lett.* **1995**, *20*, 970 – 972.
[41] D. Zeisel, S. Nettesheim, B. Dutoit, R. Zenobi, *Appl. Phys. Lett.* **1996**, *68*, 2491 – 2492.

[42] M. N. Islam, X. K. Zhao, A. A. Said, S. S. Mickel, C. F. Vail, *Appl. Phys. Lett.* **1997**, *71*, 2886 – 2888.
[43] R. Stöckle, V. Deckert, C. Fokas, R. Zenobi, B. Hecht, B. Sick, U. P. Wild, *Appl. Phys. Lett.* **1999**, *75*, 160 – 162.
[44] J. Pawley, *Handbook of Biological Confocal Microscopy*, Plenum, New York, **1995**.
[45] J. K. Trautman, J. J. Macklin, L. E. Brus, E. Betzig, *Nature* **1994**, *369*, 40 – 42.
[46] X. S. Xie, R. C. Dunn, *Science* **1994**, *265*, 361 – 364.
[47] R. C. Dunn, G. R. Holtom, L. Mets, X. S. Xie, *J. Phys. Chem.* **1994**, *98*, 3094 – 3098.
[48] X. S. Xie, J. K. Trautman, *Ann. Rev. Phys. Chem.* **1998**, *49*, 441 – 480.
[49] A. G. T. Ruiter, J. A. Veerman, M. F. Garcia-Parajo, N. F. van Hulst, *J. Phys. Chem. A* **1997**, *101*, 7318 – 7323.
[50] U. Ziegler, A. Vinckier, P. Kernen, D. Zeisel, J. Biber, G. Semenza, H. Murer, P. Groscurth, *Mol. Biol. Cell* **1998**, *9*, 600.
[51] M. K. Hong, S. Erramilli, P. Huie, G. James, A. Jeung, *SPIE* **1996**, *2863*, 54 – 63.
[52] D. P. Tsai, A. Othonos, M. Moskovits, *Appl. Phys. Lett.* **1994**, *64*, 1768 – 1770.
[53] C. L. Jahncke, M. A. Paesler, H. D. Hallen, *Appl. Phys. Lett.* **1995**, *67*, 2483 – 2485.
[54] C. L. Jahncke, H. D. Hallen, M. A. Paesler, *J. Raman Spectrosc.* **1996**, *27*, 579 – 586.
[55] D. A. Smith, S. Webster, M. Ayad, S. D. Evans, D. Fogherty, D. Batchelder, *Ultramicroscopy* **1995**, *61*, 247 – 252.
[56] S. R. Emory, S. Nie, *Anal. Chem.* **1997**, *69*, 2631 – 2635.
[57] Y. Narita, T. Tadokoro, T. Ikeda, T. Sakai, S. Mononobe, M. Ohtsu, *Appl. Spectrosc.* **1998**, *52*, 1141 – 1144.
[58] S. J. Stranick, L. J. Richter, R. R. Cavanagh, *J. Vac. Sci. Technol. B* **1998**, *16*, 1948 – 1952.
[59] D. Zeisel, B. Dutoit, V. Deckert, T. Roth, R. Zenobi, *Anal. Chem.* **1997**, *69*, 749 – 754.
[60] D. Zeisel, V. Deckert, R. Zenobi, T. Vo-Dinh, *Chem. Phys. Lett.* **1998**, *283*, 381 – 385.
[61] T. Vo-Dinh, *Surface-Enhanced Raman Scattering*, Elsevier Science, **1995**.
[62] V. Deckert, D. Zeisel, R. Zenobi, T. Vo-Dinh, *Anal. Chem.* **1998**, *70*, 2646 – 2650.
[63] R. Stöckle, V. Deckert, C. Fokas, D. Zeisel, R. Zenobi, *Vibr. Spectrosc.* **2000**, *22*, 39 – 48.
[64] M. Moskovits, *J. Mod. Phys.* **1985**, *57*, 783 – 826.
[65] K. Kneipp, Y. Wang, H. Kneipp, I. Itzkan, R. R. Dasari, M. S. Feld, *Phys. Rev. Lett.* **1996**, *76*, 2444 – 2446.
[66] G. Krausch, J. Mlynek, *Microelectron. Eng.* **1996**, *32*, 219 – 228.
[67] D. Kossakovski, S. D. O'Connor, M. Widmer, J. D. Baldeshwieler, J. L. Beauchamp, *Ultramicroscopy* **1998**, *71*, 111 – 115.
[68] J. D. Hogan, D. A. Laude, *The 38th ASMS Conference on Mass Spectrometry and Allied Topics*, Tucson, Arizona, **1990**, pp. 848 – 849.
[69] K. Dreisewerd, M. Schürenberg, M. Karas, F. Hillenkamp, *Int. J. Mass Spectrom. Ion Processes* **1995**, *141*, 127 – 148.
[70] B. Dutoit, D. Zeisel, V. Deckert, R. Zenobi, *J. Phys. Chem. B* **1997**, *101*, 6955 – 6959.
[71] M. Stähelin, M. A. Bopp, G. Tarrach, A. J. Meixner, I. Zschokke-Gränacher, *Appl. Phys. Lett.* **1996**, *68*, 2603 – 2605.
[72] H. J. Mamin, *Appl. Phys. Lett.* **1996**, *69*, 433 – 435.
[73] C. Lienau, A. Richter, T. Elsaesser, *Appl. Phys. Lett.* **1996**, *69*, 325 – 327.
[74] D. Singleton, G. Paraskevopoulos, R. S. Taylor, *Chem. Phys.* **1990**, *144*, 415 – 423.
[75] R. Stöckle, N. Schaller, V. Deckert, C. Fokas, R. Zenobi, *J. Microsc.* **1999**, *194*, 378 – 382.
[76] K. Sasaki, *J. Vac. Sci. Technol. B* **1997**, *15*, 2786 – 2790.
[77] R. Stöckle, Y.-D. Suh, V. Deckert, R. Zenobi, *Chem. Phys. Lett.* **2000**, *318*, 131 – 136.